and flatness monitor indication (FMI) are defined as

$$\overrightarrow{\mathrm{PMI}}(I_f : x, y) = \sum_{i=1}^{8} (m_f)_i \cdot \vec{r}_i(x_i, y_i) = \begin{cases} \sum_{i=1}^{8} (m_f)_i \cdot x_i \\ \sum_{i=1}^{8} (m_f)_i \cdot y_i \end{cases}$$

$$= \begin{cases} \mathrm{PMI}(I_f : x) \\ \mathrm{PMI}(I_f : y) \end{cases}, \quad |\vec{r}_i| = 1 \text{ (8 fan shape)}, \tag{1}$$

$$\begin{cases} \overrightarrow{\mathrm{FMI}}(I_f : x, y) = \sum_{j=1}^{8} (M_f)_j \cdot \vec{R}_j(x_j, y_j) = \begin{cases} \sum_{j=1}^{8} (M_f)_j \cdot x_j \\ \sum_{j=1}^{8} (M_f)_j \cdot y_j \end{cases} \\ \qquad = \begin{cases} \mathrm{FMI}(I_f : x) \\ \mathrm{FMI}(I_f : y) \end{cases}, \qquad |\vec{R}_j| = 1 \text{ (8 fan shape)}, \\ \mathrm{FMI}(I_c) = \sum_{k=1}^{8} \left| \dfrac{(M_c)_k}{(M_c)_1 \cdot (2 \cdot k - 1)} - 1 \right| \qquad \text{(8 concentric shape)}. \end{cases} \tag{2}$$

Here, i, j and k denote identification of 8 fan and concentric separated areas, respectively. m_f, M_f and M_c are output signals from each separated area. In the profile monitor, the centre and symmetry are indicated by the length of the thick vector, $\mathrm{PMI}(I_f : x, y)$ and the shape formed with 8 thin vectors, $(m_f)_j \cdot r_j$, shown in figure 2. The beam approaches a centre position of the profile monitor as the length of the thick vector shortens. Similarly, in the flatness monitor, the symmetry and flatness of the dose profile are indicated by the length of the thick vector, $\mathrm{FMI}(I_f : x, y)$, and the value of $\mathrm{FMI}(I_c)$.

2.2. Measurement of relationship between the incident beam conditions and uniformity of the dose distribution

The dose distribution optimized in an irradiation field of 200 mm ϕ by the dual-ring double-scattering method is formed by the following equations (Takada 2002):

$$F(r) = f_{\mathrm{inner}}(r) + f_{\mathrm{outer}}(r),$$

$$f_{\mathrm{inner}}(r) = 1.80 \times 10^{-9} \cdot \exp(-8.90 \times 10^{-5} \cdot r^2) \int_0^{90} k \cdot \exp(-1.89 \times 10^{-4} \cdot k^2) \times \left[\int_0^{\pi} \exp(1.78 \times 10^{-4} \cdot r \cdot k \cdot \cos\theta)\, \mathrm{d}\theta \right] \mathrm{d}k,$$

$$f_{\mathrm{outer}}(r) = 1.06 \times 10^{-8} \cdot \exp(-5.22 \times 10^{-4} \cdot r^2) \int_{90}^{\infty} k \cdot \exp(-6.22 \times 10^{-4} \cdot k^2) \times \left[\int_0^{\pi} \exp(1.04 \times 10^{-3} \cdot r \cdot k \cdot \cos\theta)\, \mathrm{d}\theta \right] \mathrm{d}k. \tag{3}$$

Here, $f_{\mathrm{inner}}(r)$ and $f_{\mathrm{outer}}(r)$ denote the dose distribution components by the inner and outer rings of the second scatter, respectively, and r denotes the distance from the centre of the beam axis. Table 1 shows the conditions of the first and second scatters at each beam energy of 150 MeV, 190 MeV and 235 MeV. To obtain a dose distribution with a high degree of uniformity in the irradiation field, stability of the beam incidence position at the dual-ring scatter is very important.

The depth and lateral dose distribution for beam energies of 150, 190, 235 MeV, each SOBP, and FD in the field size of 200 mm are measured by changing the incident beam condition in the irradiation equipment. The measurement of the dose distribution is performed using a three-dimensional (3D) water phantom and an ionization chamber with a sensitive

Figure 3. Picture of 3D water phantom.

Table 1. Thickness and characteristics of the first and second scatters.

Energy (MeV)	First scatter (Pb) thickness (mm)	Inside second scatter (Pb) thickness (mm)	Inside second scatter (Pb) diameter (mm)	Outside second scatter (Al) thickness (mm)
150	1.5	2.952	27.48	7.997
190	2.3	4.038	25.58	11.087
235	3.5	5.314	24.00	14.760

volume of 75 μl (figure 3). The 3D water phantom can rotate together with a nozzle of the rotating gantry. The depth and lateral dose distribution are measured by 1 mm and 2 mm step s^{-1}, respectively.

The uniformity of the measured lateral dose distribution was evaluated using parameters defined by the following symmetry and flatness (IEC 1989):

$$\text{Uniformity} = \begin{cases} \text{Symmetry} : S_{\text{FWHM}}\,[\%] = \dfrac{A_+ - A_-}{A_+ + A_-} \times 100, \\ \text{Flatness} : F_{0.8\times\text{FWHM}}\,[\%] = \dfrac{D_{\max} - D_{\min}}{D_{\max} + D_{\min}} \times 100. \end{cases} \tag{4}$$

The symmetry is expressed as the difference between the area on the '+' side of the lateral position (A_+) and the area on the '$-$' side of the lateral position (A_-) within an area of full-width at half-maximum (FWHM). The flatness is expressed as the difference between the maximal radiation dose ($D_{\max}$) and the minimal radiation dose ($D_{\min}$) within an area of 80% FWHM. The IEC (1989) report recommends symmetry of less than $\pm 2\%$ and flatness of less than 5%. However, the symmetry and flatness for proton radiotherapy are not regulated. In this study,

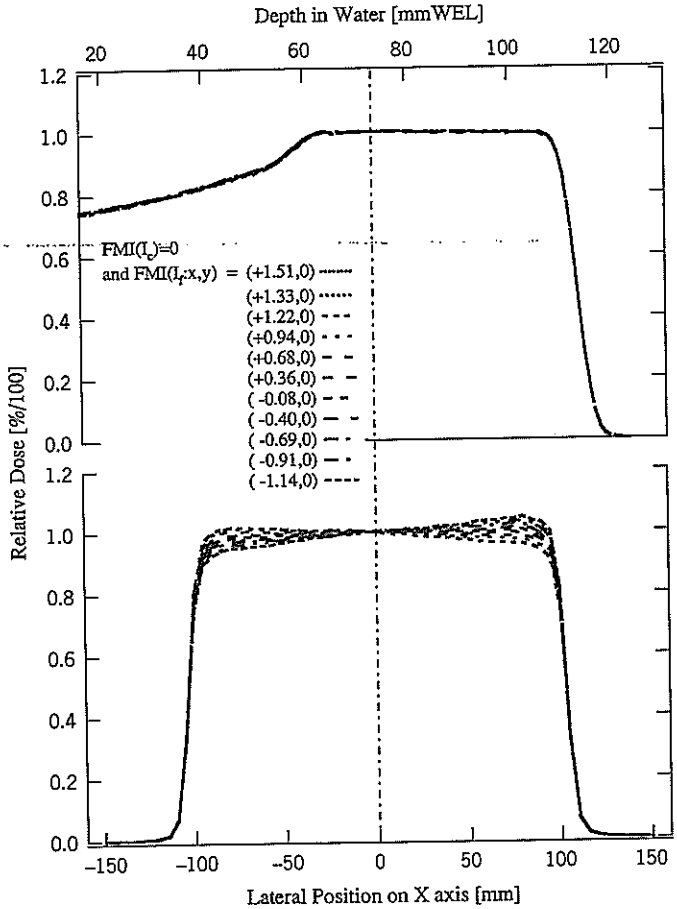

Figure 4. Depth and X-axis lateral dose distributions measured at $\overrightarrow{\mathrm{FMI}}(I_f : x, y) = (\mathrm{FMI}(I_f : x), 0)$ with $\mathrm{FMI}(I_c) \approx 0$ under the conditions of 150 MeV/SOBP 50 mm/Gantry = 0°.

we used symmetry of less than ±1% and flatness of less than 2.5% for the evaluation of proton radiotherapy.

3. Results and discussions

3.1. Correlation between the flatness monitor indication and uniformity of the dose distribution

The uniformity of the dose distribution in proton radiotherapy is observed using a flatness monitor. Figure 4 shows the depth and lateral dose distribution on the central axis of an SOBP measured at $\overrightarrow{\mathrm{FMI}}(I_f : x, y) = (-1.14, 0) \leftrightarrow (+1.51, 0)$ and $\mathrm{FMI}(I_c) \approx 0$ under the conditions of 150 MeV/SOBP 50 mm/Gantry = 0°. Figure 5 shows the symmetry and flatness of the lateral dose distribution measured at the flatness monitor indications under the conditions of 150 MeV/SOBP 50 mm/Gantry = 0°, 190 MeV/SOBP 80 mm/Gantry = 0° and 235 MeV/SOBP 80 mm/Gantry = 0°. These findings indicated that the uniformity of the dose distribution decreased by changing the $\overrightarrow{\mathrm{FMI}}(I_f : x, y)$ from the standard: $\overrightarrow{\mathrm{FMI}}(I_f : x, y) \approx (0, 0)$ and $\mathrm{FMI}(I_c) \approx 0$.

To satisfy a symmetry of less than ±1% and flatness of less than 2.5% in the dose distribution for proton radiotherapy, the $\mathrm{FMI}(I_f : x)$ and $\mathrm{FMI}(I_f : y)$ must be within ±0.03, respectively. Since no differences in the shape of the depth–dose distribution under different beam conditions were observed, it was not discussed in this study.

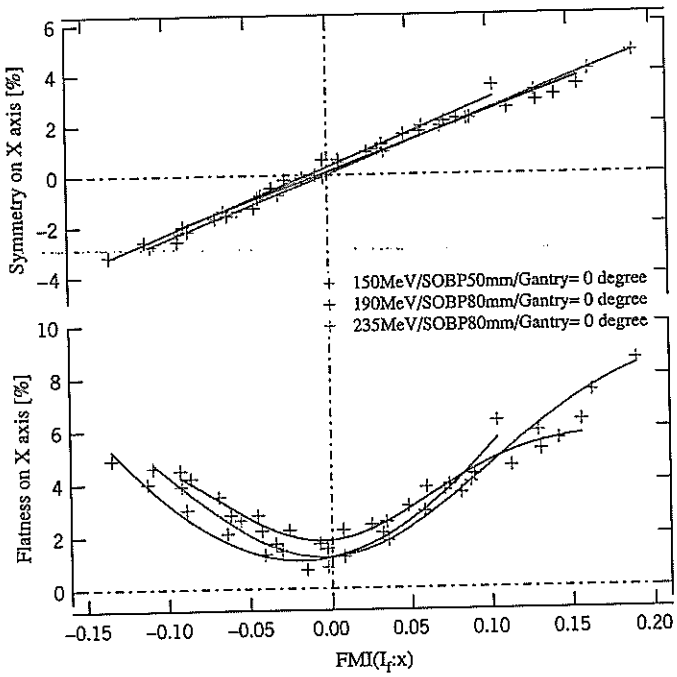

Figure 5. Symmetry and flatness of the X-axis lateral dose distribution measured at $\overrightarrow{\mathrm{FMI}}(I_f : x, y) = (\mathrm{FMI}(I_f : x), 0)$ with $\mathrm{FMI}(I_c) \approx 0$ under the conditions of 150 MeV/SOBP 50 mm/Gantry = 0°, 190 MeV/SOBP 80 mm/Gantry = 0°, and 235 MeV/SOBP 80 mm/Gantry = 0°.

3.2. Correlation between the profile monitor indication and the uniformity of the dose distribution with changes in the second scatter position

Figure 6 shows the uniformity of the dose distribution by mechanically moving the second scatter in 0.4 mm steps from the scatter position (−6 mm) with the initial beam condition for the uniform dose profile: $\overrightarrow{\mathrm{FMI}}(I_f : x, y) = (0, 0)$ and $\mathrm{FMI}(I_c) \approx 0$. Only the second scatter was moved in the constant beam condition ($\overrightarrow{\mathrm{FMI}}(I_f : x, y) \neq (0, 0)$). The movement value of the second scatter corresponded to the difference between the positions of the second scatter centre and the large Gaussian beam centre passing through the first scatter by the principle of the dual-ring double-scattering method. The uniformity of the dose distribution for proton radiotherapy is satisfied when the difference is less than 1 mm between the positions of the second scatter centre and the beam centre axis.

3.3. Correlation between the second scatter position and the profile monitor indication

The top graph of figure 7 shows the correlation between the incidence position of the beam observed by the profile monitor and the second scatter position. The second scatter was moved in a plane perpendicular to the beam axis so that the $\overrightarrow{\mathrm{FMI}}(I_f : x, y) = (0, 0)$ to the incidence beams. In the range of $|\overrightarrow{\mathrm{PMI}}(I_f : x, y)| \leqslant (1.0, 1.0)$, there was a linear correlation between the positions of the second scatter and incidence beams.

The middle and bottom graphs show the symmetry and flatness of the dose distribution with the second scatter position evaluated using equation (3). The results shown in figure 7 indicated that the flatness of the dose distribution required the $|\overrightarrow{\mathrm{PMI}}(I_f : x, y)| < (0.5, 0.5)$ and the second scatter position of 3–7 mm. The changes in the symmetry and flatness of the dose distribution caused by moving the second scatter were slower than those shown in figure 6. The beam centre always matches with the second scatter centre by movement

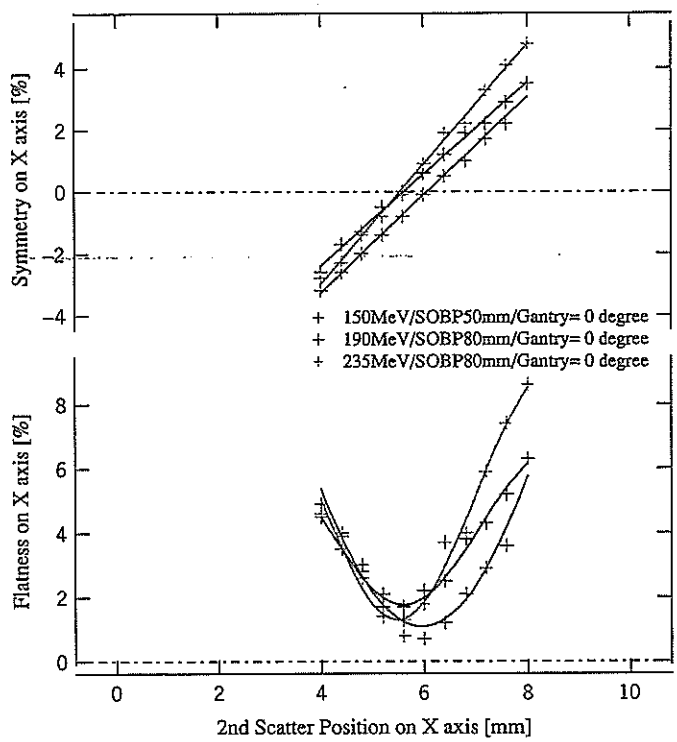

Figure 6. Symmetry and flatness of the X-axis lateral dose distribution by moving the second scatter under the conditions of 150 MeV/SOBP 50 mm/Gantry = 0°, 190 MeV/SOBP 80 mm/Gantry = 0°, and 235 MeV/SOBP 80 mm/Gantry = 0°.

of the second scatter position with $\overrightarrow{\mathrm{FMI}}(I_f : x, y) = (0, 0)$ in figure 7, but not with $\overrightarrow{\mathrm{FMI}}(I_f : x, y) \neq (0, 0)$ in figure 6. This indicated that the relationship of the relative position between the second scatter centre and beam axis centre was very important. In the stability of the beam from the proton accelerator, C235, since the irradiated beam conditions were not changed by $|\overrightarrow{\mathrm{FMI}}(I_f : x, y)| > (0.03, 0.03)$ during beam irradiation within about 10 min, the $\overrightarrow{\mathrm{FMI}}(I_f : x, y)$ always indicated a level close to zero during the proton treatment.

3.4. Control method for highly accurate uniformity of the dose distribution during proton treatment

To obtain uniformity of the dose distribution in the irradiation field by the dual-ring double-scattering method, the incident beam must satisfy strict conditions. If the central axis of beams moves more than 1 mm from the centre of the second scatter, the uniformity of the irradiation field becomes lower than the clinically useful level. The central axis of beams must be within the circle with a radius of 1 mm from the centre of the second scatter. In our institution, since changes in the beam axis during proton irradiation of less than 1 min for treatment are very small, there are no problems in maintaining uniformity of the dose distribution in the irradiation field if the central axis of beams is adjusted to agree with the centre of the second scatter before each irradiation. However, daily or long-term changes in the beams are larger than the accuracy required for the treatment, affecting the uniformity of the dose distribution.

To obtain highly accurate uniformity of the dose distribution in the irradiation field during proton radiotherapy, we developed a control system, consisting of functions for automatic fine adjustment of the central axis of beams and for placing the centre of the second scatter on the central axis of beams by moving the scatter mechanically. The central axis of beams is adjusted from the side closer to the beam source, brought about by a combination of the

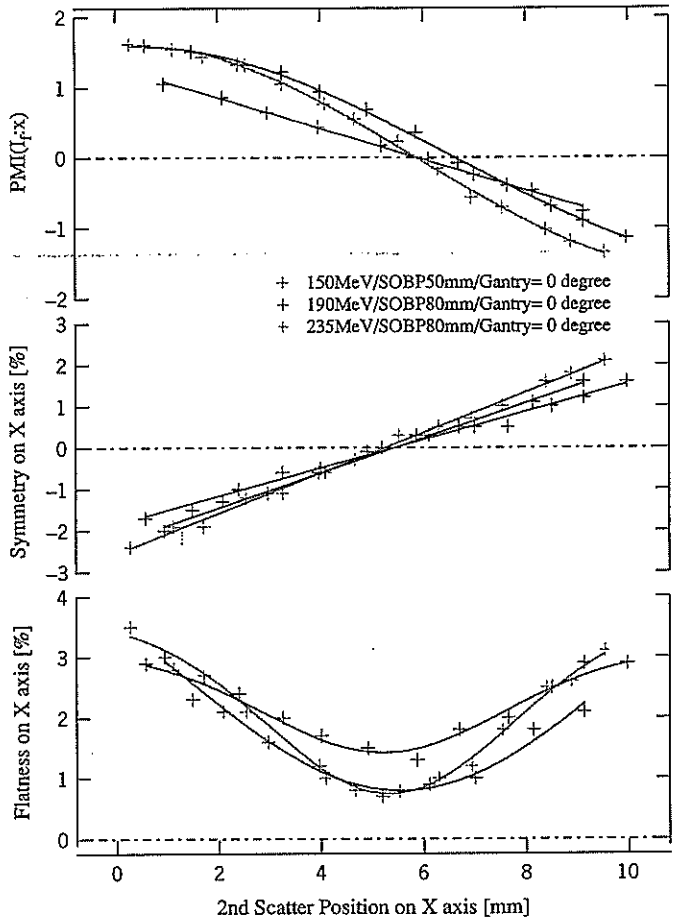

Figure 7. $\overrightarrow{\mathrm{PMI}}(I_f : x, y) = (\mathrm{PMI}(I_f : x), 0)$, symmetry, and flatness of the X-axis lateral dose distribution with respect to the position of the second scatter under the conditions of 150 MeV/SOBP 50 mm/Gantry = 0°, 190 MeV/SOBP 80 mm/Gantry = 0° and 235 MeV/SOBP 80 mm/Gantry = 0°.

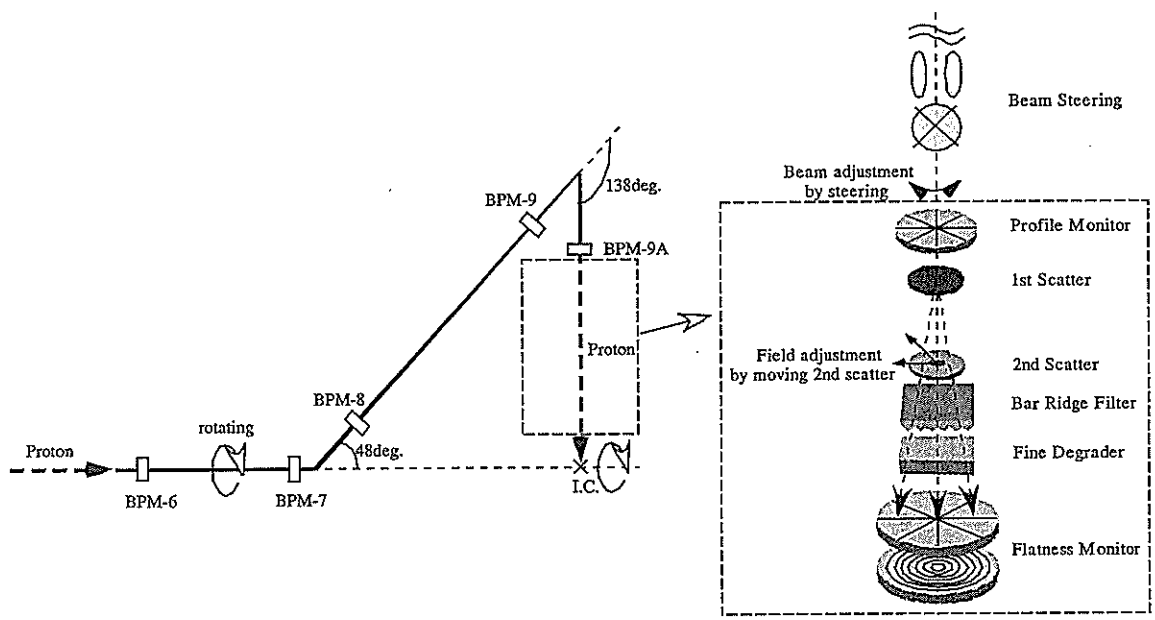

Figure 8. Arrangement of the beam profile monitor fixed in the rotating gantry and the outline of the irradiation apparatus for control of uniformity of the dose distribution at high accuracy.

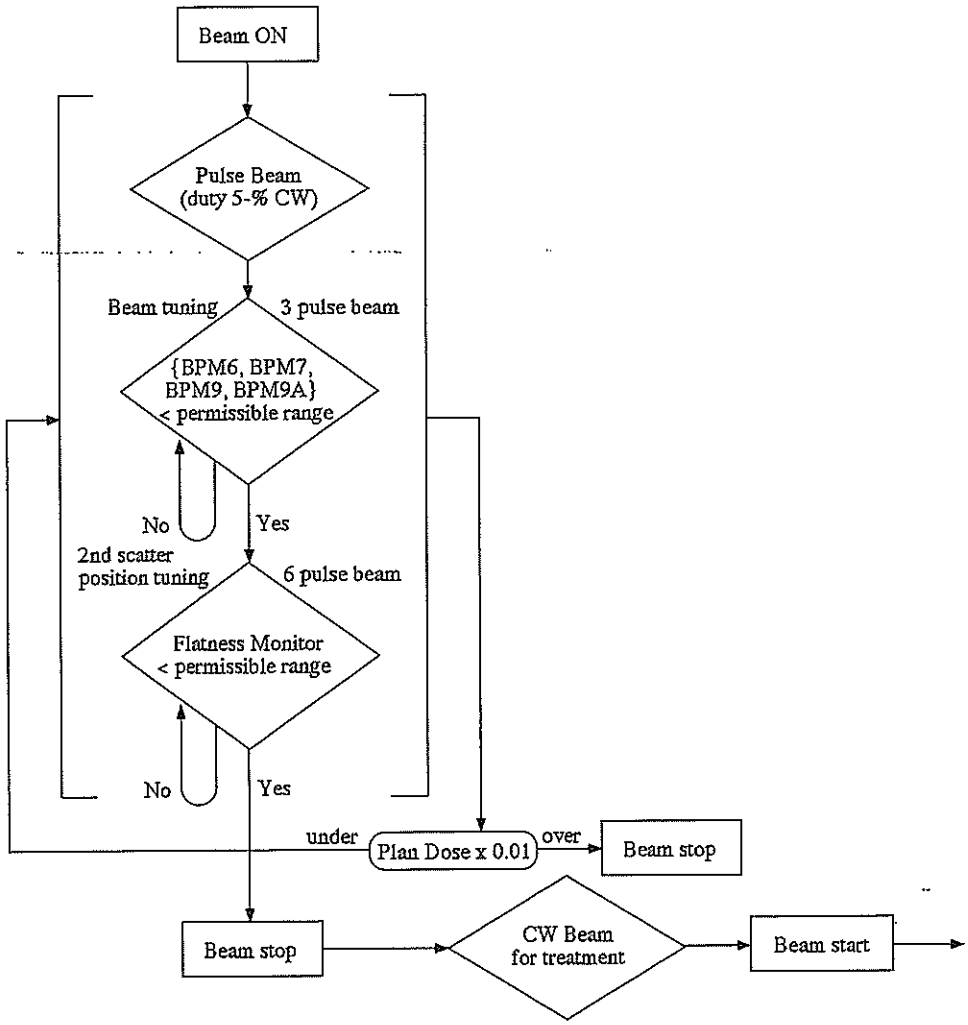

Figure 9. Flowchart of the control procedures for uniformity of the dose distribution at high accuracy.

beam profile monitor (BPM) fixed on the beam transport system of the rotating gantry and the steering electromagnet. The centre of the second scatter is adjusted to agree with the central axis of the incident beam by the profile and flatness monitors built into the irradiation apparatus (figure 8). After positioning the patient for treatment, the adjustment is performed by delivering pulsed proton beams to the patient with the settings for the treatment conditions prescribed for the patient, which is completed by an irradiation of less than 1% of the administration dose. Figure 9 shows the flowchart of the control procedures.

3.5. Results of the dose distribution uniformity by beams used in proton treatment

Figure 10 shows the characteristics of the correlation between the profile monitor indication and the centre of the second scatter under different conditions of proton irradiation after control of the dose distribution at high accuracy. In the figures obtained at the proton beam energies of 150 MeV, 190 MeV and 235 MeV, the symbols indicate all data for the condition of the SOBP width, the thickness of FD, the field size and the angle of the rotating gantry used in clinical treatment.

Taking the characteristics shown in figure 7 into consideration, the uniformity of the proton dose distribution in the irradiation field during treatment was at a level indicated by a symmetry of less than $\pm 1\%$ and flatness of less than 2%.

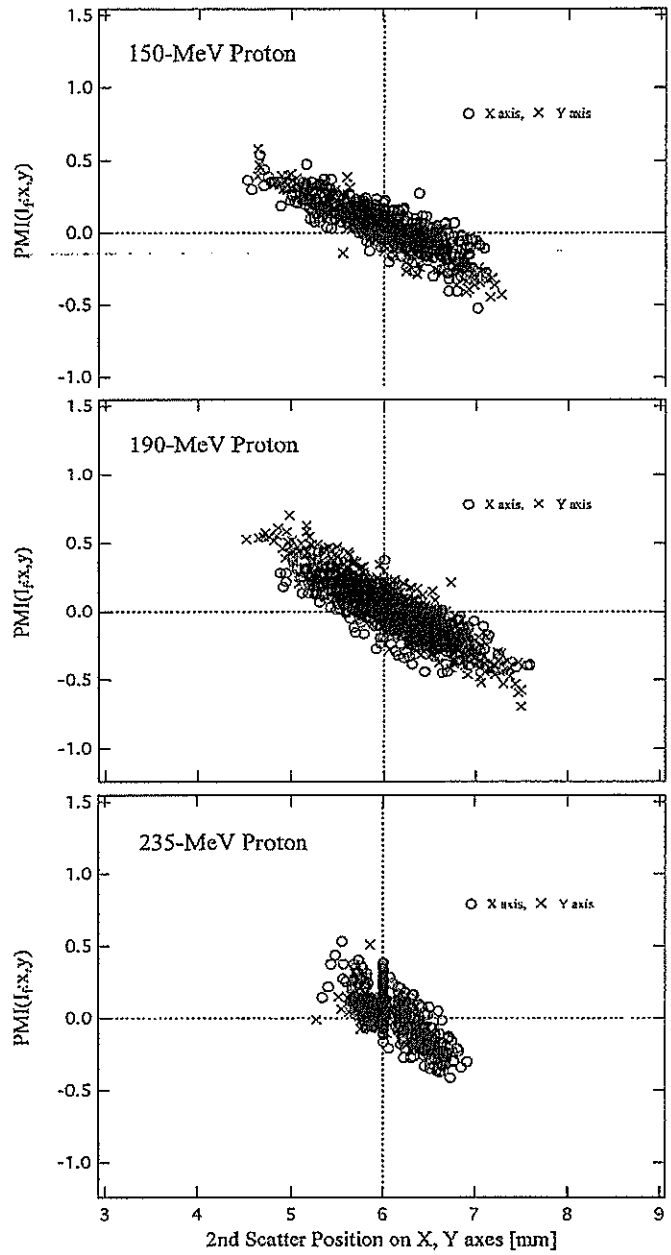

Figure 10. Characteristics of the correlation between the $\overrightarrow{\mathrm{PMI}}(I_f : x, y)$ and the centre of the second scatter after control of the dose distribution at high accuracy under different conditions of proton irradiation used in clinical treatment.

4. Conclusions

It is very difficult to obtain uniformity of the dose distribution in the irradiation field during proton radiotherapy by the dual-ring double-scattering method. Uniformity of the dose distribution during treatment could be obtained at high accuracy by using the control method that we developed. To adjust the central axis of beams to be within a circle with a radius of 1 mm, a high performance electromagnet and its power source would be required. Apparatus for proton radiotherapy with uniformity of the dose distribution at high accuracy can be provided to facilities to be built in the future at low costs using this control method.

Acknowledgments

We would like to thank the staff members of the Proton Radiotherapy Department of National Cancer Center Hospital East for help, the members of SHI Accelerator Service Ltd for the development of the apparatus, and the members of SHI Accelerator Service Ltd and Accelerator Engineering Inc. for the operation of the proton apparatus.

References

Chu W T, Ludewigt B A and Renner T R 1993 Instrumentation for treatment of cancer using proton and light-ion beams *Rev. Sci. Instrum.* **64** 2055–122

Graffman S, Jung B and Larsson B 1973 Design studies for a 200 MeV proton clinic for radiotherapy *6th Int. Cyclotron Conf. (Am. Inst. Phys., Vancouver, 1972)* vol 9 pp 603–15

IEC (International Electrotechnical Commission) 1989 *Medical Electrical Equipment*

Koehler A M, Schneider R J and Sisterson J M 1977 Flattening of proton dose distribution for large-field radiotherapy *Med. Phys.* **4** 297–301

Nishio T 1999 Present status and planning of facilities for proton and heavy ion cancer treatment in Japan—National Cancer Center *J. At. Energy Soc.* **41** 1134–8

PTCOG Newsletter 2004 PARTICLES 34 (July)

Tachikawa T, Sato T, Ogino T and Nishio T 1999 Proton treatment devices at National Cancer Center (Kashiwa, Japan) *Radiat. Indust.* **84** 48–53

Takada Y 1994 Dual-ring double scattering method for proton beam spreading *Japan. J. Appl. Phys.* **33** 353–9

Takada Y 2002 Optimum solution of dual-ring double scattering system for an incident beam with given phase space for proton beam spreading *Nucl. Instrum. Methods* A **485** 255–76

Clinical Outcomes of Single-Fraction Stereotactic Radiation Therapy of Lung Tumors

Ryusuke Hara, M.D.
Jun Itami, M.D.
Tatsuya Kondo, M.D.
Takashi Aruga, M.D.
Takashi Uno, M.D.
Nakashi Sasano, M.D.
Kayoko Ohnishi, M.D.
Makoto Kiyozuka, M.D.
Masashi Fuse, R.T.T.
Masashi Ito, R.T.T.
Kuniji Naoi, R.T.T.
Yuzuru Kohno, R.T.T.

Department of Radiation Therapy and Oncology, International Medical Center of Japan, Tokyo, Japan.

Presented in part at the 45th Annual Meeting of the American Society for Therapeutic Radiology and Oncology, Salt Lake City, Utah, October 20–23, 2003.

Address for reprints: Jun Itami, M.D., Department of Radiation Therapy and Oncology, International Medical Center of Japan, Toyama 1-21-1, Shinjyuku-ku, 162-8655 Tokyo, Japan; Fax: (011) 81 3 3207-1038; E-mail: jitami@imcj.hosp.go.jp

Received April 26, 2005; revision received September 19, 2005; accepted October 13, 2005.

BACKGROUND. The objective of the current study was to investigate the effects and the morbidities of single-fraction stereotactic radiation therapy (SRT) for lung tumors.

METHODS. A Microtron device was modified to deliver stereotactic irradiation under respiratory gating. Between August 1998 and December 2004, 59 malignant lung tumors (11 primary tumors, 48 metastases) that measured < 40 mm in greatest dimension were treated by single-fraction SRT. Nine tumors received a minimal dose of < 30 grays (Gy), and 50 tumors received a minimal dose of ≥ 30 Gy. The macroscopic target volume ranged from 1 cc to 19 cc (mean, 5 cc).

RESULTS. The 1-year and 2-year local progression-free rates (LPFRs) were 93% and 78%, respectively. The overall survival rate was 76.5% at 1 year and 41% at 2 years. Local regrowth of the irradiated tumor was a direct cause of death in two patients. Only the minimal radiation dose to the reference target volume tended to have an influence on the LPFR ($P = 0.068$). The 2-year LPFRs for patients who received irradiation doses of ≥ 30 Gy and < 30 Gy were 83% and 52%, respectively. With regard to morbidities, Grade 3 respiratory symptoms (according to the Radiation Therapy Oncology Group/European Organization for Research and Treatment of Cancer late radiation morbidity scoring scheme) were noted in one patient.

CONCLUSIONS. The results from the current study suggested that single-fraction SRT was tolerable and was capable of attaining excellent local control in patients who had malignant lung tumors that measured < 4 cm in greatest dimension. *Cancer* 2006;106:1347–52. © *2006 American Cancer Society.*

KEYWORDS: stereotactic radiation therapy, lung tumor, single fraction, respiratory gating.

Recently, wide applications have been identified for stereotactic radiation therapy (SRT) in the treatment of solid tumors, especially lung and liver tumors. In localized tumors, favorable results comparable to those achieved with surgical intervention were obtained with hypofractionated SRT.[1–4] From the standpoint of normal tissue tolerance, single, high-dose irradiation is prohibitive. With the advent of SRT, it has been demonstrated that single, high-dose irradiation is tolerable if the planning target volume (PTV) is very small and if radiation therapy is delivered by 3-dimensional (3-D), converging, noncoplanar arcs. This single-fraction, high-dose radiation therapy is administered mainly to intracranial tumors. Therefore, it presumably is possible to extrapolate that the same single-fraction, high-dose irradiation can be delivered to lung tumors provided that the PTV is small enough and that radiation therapy is delivered by 3-D, noncoplanar, converging beams. However, to our knowledge, there are only a few reports to date regarding the use of SRT with a single

DOI 10.1002/cncr.21747
Published online 10 February 2006 in Wiley InterScience (www.interscience.wiley.com).

fraction, and the optimal single-fraction dose for controlling local tumor remains to be established.[5,6]

We have developed a Microtron-based system for SRT of solid tumors that delivers radiation at a predetermined respiratory phase.[7] Patients with lung tumors have been treated by a single-fraction SRT using this system since August 1998.[8] In this article, we report the outcomes of their treatment.

MATERIALS AND METHODS

A Microtron device (Hitachi Medical Co., Tokyo, Japan) was modified to deliver SRT of 6-megavolt X-rays under respiratory gating. The detailed descriptions of the system and the treatment method have been reported elsewhere.[7,8] Briefly, a custom-made fixing cradle is made for each patient, and computed tomography (CT) simulation in an end-expiratory phase is performed with the patient lying in the cradle. Multiportal, noncoplanar radiation treatment is planned and evaluated by using dose-volume histograms. The portals range in number from 9 to 16 (mean, 13 portals). Respiratory movement of the chest wall is measured continuously by a laser displacement monitor (Keyence, Tokyo, Japan) placed over the patient's chest. The monitor is able to detect distance changes > 0.5 mm between the monitor and the chest wall surface. The obtained respiratory movements of the chest wall are sent to the respiratory gating system, where on signals for irradiation are delivered to the Microtron at an arbitrary respiratory phase. The actual radiation therapy is delivered with the Microtron only at the end-expiratory phase.

Between August 1998 and December 2003, 59 malignant peripheral lung tumors that measured < 40 mm in greatest dimension (7 tumors measured > 30 mm in greatest dimension) were treated by single-fraction SRT after informed consent was obtained from all patients. Six patients were irradiated twice, and three patients were irradiated 3 times: Therefore, there were 47 patients in total. The female-to-male ratio was 9:38, and the mean patient age was 67 years. The majority of lung tumors (48 of 59 tumors; 81%) were metastatic lesions from various primary sites. The primary tumor site was the lung in 11 tumors, the colon in 9 tumors, the head and neck in 9 tumors, and the liver in 6 tumors. Eleven tumors were primary lung carcinomas, only 4 of which were TNM Stage I tumors.[9] Among the remaining seven primary lung carcinomas, only primary lesions were treated by SRT, and coexistent mediastinal and/or metastatic lesions were managed by other modalities. Histologically, 27 tumors were adenocarcinomas and 15 tumors were squamous cell carcinomas. All four Stage I primary lung carcinomas were adenocarcinomas. Three histologically unknown tumors were included in the current study, because radiologic studies, which included fluorodeoxyglucose-positron emission tomography (FDG-PET), strongly indicated the malignant nature of those lesions.

The macroscopic tumor volume (GTV)[10] ranged from 1 cc to 19 cc (mean, 5 cc). In this study, we assumed that the clinical target volume (CTV) was equal to the GTV displayed by CT images of the lung field windows. For the PTV, 5-mm margins were taken into account in all directions from the CTV. Before December 2001, the prescribed dose was calculated by using the minimal dose of the GTV = CTV as a reference target volume (29 tumors). Thereafter, the prescribed dose was calculated as the minimal dose to the PTV (30 tumors). Nine tumors received the minimal dose of 20 grays (Gy) or 25 Gy, and 50 tumors received ≥ 30 Gy (range, 30–34 Gy).

In 32 tumors, respiratory gating was not performed. In 9 of those 32 tumors, respiratory cycles were too irregular for the system to determine the end-expiratory phase. In the remaining 23 tumors, respiratory gating was not necessary because the ranges of tumor movement by respiration were < 5 mm (Table 1).

After the completion of SRT, CT scans were obtained bimonthly for up to at least 6 months and were evaluated according to the Response Evaluation Criteria in Solid Tumors.[11] A complete response (CR) was defined as the disappearance of all target lesions. A partial response (PR) was defined as a decrease $\geq 30\%$ in the sum of the greatest dimensions of the target lesions by using the baseline greatest dimension sum as the reference. Progressive disease (PD) was defined as an increase $\geq 20\%$ in the sum of the greatest dimension of the target lesions using the smallest sum of the greatest dimension recorded since the initiation of treatment or since the appearance of ≥ 1 new lesion as the reference point. Stable disease (SD) was defined as neither sufficient shrinkage to qualify for a PR nor sufficient increase to qualify for PD.

The influence of each prognostic factor on the maximal response of the tumor was tested by using a Student t test for continuous variables and a chi-square test for categorical variables. The local progression-free rate (LPFR) was calculated using the Kaplan–Meier method[12] assuming regrowth of the irradiated tumor as an event, irrespective of the status of other lesions outside of the treatment volume. A tumor was censored in patients who died without tumor regrowth. Differences between LPFR curves were tested by using the log-rank method.

TABLE 1
Patient, Target, and Treatment Characteristics

Characteristic	No. of patients
Gender (no.)	
Male	38
Female	9
Age	
Range	32–90 yrs
Mean	67 yrs
Primary tumor site	
Lung (primary site)	11
Lung (metastatic site)	11
Colon	9
Head and neck	9
Liver	6
Esophagus	2
Breast	2
Uterus	4
Others	5
No. of target lesions	
1	38
2	6
3	3
Histology	
Adenocarcinoma	27
SCC	15
HCC	6
Others	8
Unknown	3
GTV	
Range	1–19 cc
Mean	5 cc
Minimal dose	
< 30 Gy	9
≥ 30 Gy	50
Range	20–34 Gy
Mean	30 Gy
Respiratory gating	
Yes	27
No	32
Reference volume	
GTV	29
PTV	30

SCC: squamous cell carcinoma; HCC: hepatocellular carcinoma; GTV: (gross) macroscopic tumor volume; Gy: grays; PTV: planning target volume.

For the evaluation of radiation-induced morbidities, Radiation Therapy Oncology Group/European Organization for Research and Treatment of Cancer late radiation morbidity scoring schemes[13] were used. The mean follow-up for all patients was 12 months (range, 2–42 mos).

RESULTS

In terms of the maximal response, a CR was achieved in 18 tumors, a PR was achieved in 29 tumors, and SD was achieved in 12 tumors. Regrowth was noted in 3 of 9 tumors that received radiation doses < 30 Gy (2 tumors that achieved SD and 1 tumor that achieved a PR) and in 5 of 50 tumors that received radiation doses ≥ 30 Gy (1 tumor that achieved SD, 3 tumors that achieved a PR, and 1 tumor that achieved a CR) (Table 2). All local tumor regrowth occurred within 2 years after SRT.

TABLE 2
Tumor Maximal Response and Regrowth

	Minimal dose				
	< 30 Gy		≥ 30 Gy		
Response	Regrowth	No regrowth	Regrowth	No regrowth	Total
CR	0	2	1	15	18
PR	1	4	3	21	29
NC	2	0	1	9	12
Total	3	6	5	45	59

Gy: grays; CR: complete response; PR: partial response; NC: no change.

TABLE 3
Correlation with Maximal Response: Complete and Partial Responses versus Stable Disease

Characteristic	*P* value
Gender[a]	NS
Age[b]	NS
Primary tumor site[a]	NS
Histology[a]	NS
GTV (cc)[b]	NS
Minimal dose (< 30 Gy vs. ≥ 30 Gy)[a]	NS
Respiratory gating[a]	0.02
Reference volume[a]	0.04

NS: not significant; GTV: (gross) macroscopic tumor volume; Gy: grays.
[a] Determined according to the chi-square test.
[b] Determined according to the Student *t* test.

Both demographic and clinical factors were analyzed with respect to maximal tumor response, including patient gender, patient age, primary tumor site, histology, GTV, use of respiratory gating, minimal dose, and the nature of the reference target volume. A statistically significant correlation was found between the maximal response and the use of respiratory gating and reference target volumes. A response (CRs and PRs) was obtained more frequently in the tumors without respiratory gating ($P < 0.02$) and in the tumors that were irradiated using the PTV as a reference target volume ($P < 0.04$) (Table 3).

The 1-year and 2-year LPFRs were 93% and 78%, respectively. The same demographic and clinical factors were tested with respect to their impact on LPFR.

TABLE 4
Correlations with Local Progression-Free Rate

Characteristic	*P* value[a]
Gender	NS
Age (≥ 67 yrs vs. < 67 yrs)	NS
Primary tumor site (lung primary vs. others)	NS
Histology (adenocarcinoma vs. others)	NS
GTV (> 5 cc vs. ≤ 5 cc)	NS
Minimal dose (< 30 Gy vs. ≥ 30 Gy)	0.068
Respiratory gating	NS
Reference volume	NS

NS: not significant; GTV: (gross) macroscopic tumor volume; Gy: grays.
[a] Determined according to the log-rank test.

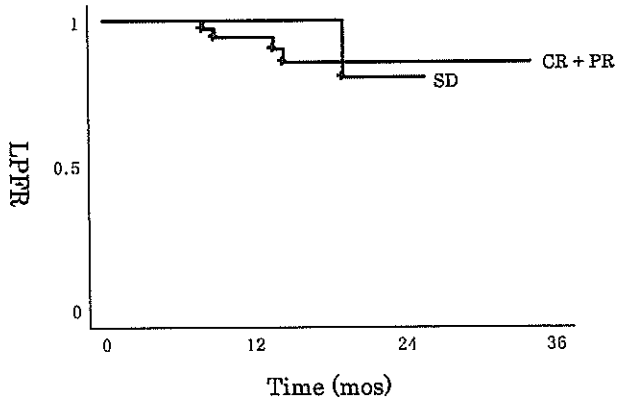

FIGURE 1. The local progression-free rate (LPFR) is illustrated according to the minimal radiotherapy dose. CR: complete response; PR: partial response; SD: stable disease.

Only the minimal dose tended to have an influence on the LPFR ($P = 0.068$) (Table 4). The 2-year LPFR for tumors that were irradiated at doses ≥ 30 Gy and < 30 Gy was 83% and 52%, respectively (Fig. 1). Excluding 9 tumors that were irradiated at doses < 30 Gy, the LPFR was calculated according to the maximal response. The 2-year LPFR for responding tumors (CRs and PRs) and for tumors that achieved SD was 85% and 80%, respectively. The difference was not found to be statistically significant (Fig. 2).

The overall survival rate was 76.5% at 1 year and 41% at 2 years. Local regrowth of the irradiated tumor was a direct cause of death in two patients.

With regard to morbidities, Grade 2 respiratory symptoms were reported in one patient. Another patient who had active tuberculosis and idiopathic interstitial pneumonia developed Grade 3 respiratory morbidities that necessitated oxygen supplement. In two patients who had subpleural tumors, skin erythema was noted and was healed without any scarring. All other tumors were treated without any incidents of acute or chronic morbidity.

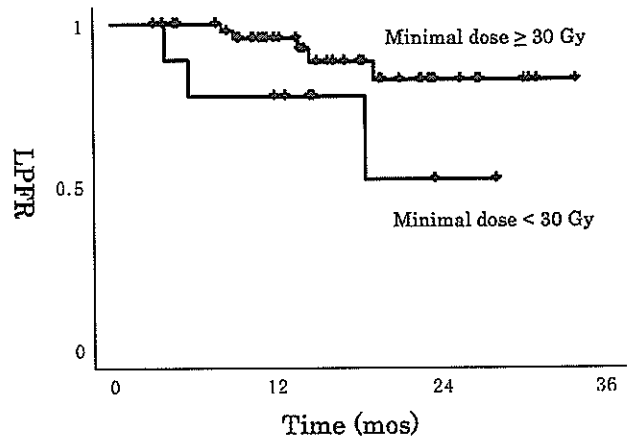

FIGURE 2. The local progression-free rate (LPFR) is illustrated according to the maximal response (minimal radiotherapy dose ≥ 30 grays [Gy]).

DISCUSSION

Single, high-dose irradiation long has been considered prohibitive because of late radiation morbidities. Even as early as the 1920s, German groups published reports of the disastrous effects of single, high-dose irradiation on normal tissues.[14] However, the very confined treatment volumes obtained with SRT has made it possible to apply a single, high dose without causing late morbidities, even in sensitive organs such as the central nervous system.[15] Single-fraction SRT is a promising modality that has the potential to circumvent the problem of repopulation, which can occur during conventional, fractionated radiation therapy, and to improve the local control of lung tumors.[6] However, to our knowledge only a few authors to date have reported results from studies that used single-fraction SRT to lung tumors. Hof et al.[5] reported on 10 patients with histologically confirmed, Stage I, non-small cell lung carcinoma who received treatment with single-fraction SRT (isocenter dose range, 19–26 Gy). After 12 months and 24 months, the local recurrence-free survival rate in their study reached 88.9% and 64%, respectively. Wulf et al.[6] reported results from a study of single-dose SRT to 25 lung metastases with a CTV < 25 cc, and no local recurrences were observed at a median follow-up of 9 months (range, 2–37 mos). In that series, the PTV was defined as the CTV plus 5–10 mm margins and was enclosed by 20.8 Gy.

In the current series, all tumors that were irradiated at a dose < 30 Gy used minimal dose of the CTV,

and not the PTV, as the prescribed dose. Therefore, in some tumors, the minimal dose to the PTV may have been lower compared with the series reported by Wulf et al. The poor 2-year LPFR of 52% noted among tumors that were irradiated at a dose < 30 Gy in the current series may have been because of the lower dose. Conversely, tumors that were irradiated at a minimal dose ≥ 30 Gy demonstrated an LPFR of 83% and, when considering only tumors that were irradiated at a dose ≥ 30 Gy by using the prescribed dose to the PTV, the 2-year LPFR reached 90%, a rate that is comparable to the results reported by Wulf et al.[5] and Hof et al.[6]

The optimal dose for the control of lung tumors by single-fraction SRT is unclear. Wulf et al. revealed a dose-response relation with an advantage for higher doses of SRT in three fractions.[6] Ohnishi et al.[4] evaluated 245 patients with Stage I nonsmall cell lung carcinoma who underwent hypofractionated SRT in Japan with a linear quadratic model[16] and found that patients who received a biologically effective dose (BED) ≥ 100 Gy at the isocenter achieved better local control and had better survival rates compared with patients who received a BED < 100 Gy. However, the linear quadratic model is not appropriate for radiotherapy with a fractionated dose > 8 Gy.[17] Therefore, it is difficult to compare single-fraction radiotherapy with multifraction radiotherapy. Although a statistically significant difference was not reached, the results of the current study demonstrated that patients who had tumors that were irradiated at a dose ≥ 30 Gy tended to have more favorable outcomes. Currently, it is preferable to use a minimal dose of 30 Gy in a single fraction to obtain good local control in patients who have malignant tumors that measure < 4 cm in greatest dimension. To our knowledge, it is unknown whether larger doses are beneficial in improving tumor control further, and the possibility for incremental dose increases also depends on the morbidities caused by single-fraction SRT.

The incidence of adverse reactions to single-fraction SRT was very low, as expected and as reported in other series.[5,6] The only Grade 3 respiratory morbidities noted in the current series were reported in a patient who had active tuberculosis and lung fibrosis. However, when an increase in the single-fraction dose is attempted, even by using stereotactic, converging X-ray beams, an increment of the dose to the healthy lung tissue is inevitable. In conventionally fractionated radiation therapy, a volume ≥ 20 Gy (V20) of irradiated lung is related closely to the incidence and severity of radiation pneumonitis.[18,19] Likewise, we used a volume of irradiated lung ≥ Gy (V8) as an indicator of radiation pneumonitis in single-fraction SRT.[20] It is mandatory to correlate such indicators with the incidence of adverse reactions to single-fraction SRT in the treatment of patients with lung tumors.

In the current study, patients who had tumors that were irradiated without respiratory gating and with PTV used as the reference volume achieved responses (CR and PR) more frequently, although the nature of the maximal response demonstrated no statistically significant influence on the LPFR. In some patients, the appearance of consolidation around the tumor by radiation pneumonitis may prevent the correct diagnosis of tumor shrinkage, and such patients may be classified erroneously with SD. The limited value of CT diagnosis in radiation response of lung tumors has been reported previously.[21] For the early prediction of local control by SRT, FDG-PET studies may be useful.[22]

The results of the current series demonstrated that single-fraction SRT may be performed safely with excellent local control in patients with lung tumors that measure < 4 cm in greatest dimension. However, longer follow-up will be required to establish the optimal dose with this method.

REFERENCES

1. Uematsu M, Shioda A, Suda A, et al. Computed tomography-guided frameless stereotactic radiography for Stage I non-small-cell lung cancer: 5-year experience. *Int J Radiat Oncol Biol Phys.* 2001;51:666–670.
2. Nagata Y, Negoro Y, Aoki T, et al. Clinical outcomes of 3D conformal hypofractionated single high-dose radiotherapy for one or two lung tumors using a stereotactic body frame. *Int J Radiat Oncol Biol Phys.* 2002;52:1041–1046.
3. Fukumoto S, Shirato H, Matsuzawa T, et al. Small-volume image-guided radiotherapy using hypofractionated, coplanar, and noncoplanar multiple fields for patients with inoperable stage I non small cell lung carcinomas. *Cancer.* 2002; 95:1546–1553.
4. Ohnishi H, Araki T, Shirato H, et al. Stereotactic hypofractionated high-dose irradiation for Stage I nonsmall cell lung carcinoma, clinical outcomes in 245 subjects in a Japanese Multiinstitutional study. *Cancer.* 2004;101:1623–1631.
5. Hof H, Herfarth KK, Munter M, et al. Stereotactic single-dose radiotherapy Stage I non-small lung cancer (NSCLC). *Int J Radiat Oncol Biol Phys.* 2003;56:335–341.
6. Wulf J, Haeddinger U, Oppitz U, et al. Stereotactic radiotherapy for primary lung cancer and pulmonary metastases: a non-invasive treatment approach in medically inoperable patients. *Int J Radiat Oncol Biol Phys.* 2004;60:186–196.
7. Hara R, Itami J, Kondo T, et al. Development of stereotactic irradiation system of body tumors under respiratory gating [in Japanese]. *Nippon Igaku Hoshasen Gakkai Zasshi.* 2002; 62:156–160.
8. Hara R, Itami J, Kondo T, et al. Stereotactic single high dose irradiation of lung tumors under respiratory gating. *Radiother Oncol.* 2002;63:159–63.

9. Sobin LH, Wittekind C. Lung and pleural tumors. In: Sobin LH, Wittekind C, editors. TNM classification of malignant tumors, 5th ed. New York: John Wiley & Sons, 1997:91–100.
10. International Commission on Radiation Units and Measurements (ICRU). Report 62: prescribing, recording and reporting photon beam therapy. Supplement to ICRU Report 50. Bethesda, MD: ICRU Publications, 1999.
11. Therasse P, Arbuck SG, Eisenhauer EA, et al. New guidelines to evaluate the response to treatment in solid tumors. European Organization for Research and Treatment of Cancer, National Cancer Institute of the United States, National Cancer Institute of Canada. *J Natl Cancer Inst.* 2000;92:205–216.
12. Kaplan L, Meier P. Nonparametric estimation from incomplete observations. *J Am Stat Assoc.* 1958;53:457–481.
13. National Cancer Institute. Common toxicity criteria, version 2.0. Bethesda, MD: National Institutes of Health, 1999.
14. Wintz H. Enfahrungen mit der Rontgentherapie der Krebse ander Erlanger Frauenklinik. *Stahlenther.* 1923;15:770–781.
15. Voges J, Treuer H, Sturm V, et al. Risk analysis of linear accelerator radiosurgery. *Int J Radiat Oncol Biol Phys.* 1996; 36:1055–1063.
16. Fowler JF. The linear-quadratic formula and progress in fractionated radiotherapy. *Br J Radiol.* 1989;62:679–694.
17. McBride W, Withers H. Biologic basis of radiation therapy. In: Perez A, Brady W, Halperin C, Schmidt-Ullrich R. editors. Principle and practice of radiation oncology. 4th ed. Philadelphia: Lippincott Williams & Wilkins, 2004:96–136.
18. Graham MV, Purdy JA, Emami B, et al. Clinical dose-volume histogram analysis non-small cell lung cancer (MSCLC). *Int J Radiat Oncol Biol Phys.* 1999;45:323–329.
19. Tsujino K, Hirota S, Endo M, et al. Predictive value of dose-volume histogram for predicting radiation pneumonitis after concurrent chemoradiation for lung cancer. *Int J Radiat Oncol Biol Phys.* 2003;55:110–115.
20. Hara R, Itami J, Komiyama T, et al. Serum levels of KL-6 for predicting the occurrence of radiation pneumonitis after stereotactic radiotherapy for lung tumors. *Chest.* 2004;125: 340–344.
21. Aoki T, Nagata Y, Negoro Y, et al. Evaluation of lung injury after three-dimensional conformal stereotactic radiation therapy for solitary lung tumors: CT appearance. *Radiology.* 2004;230:101–108.
22. MacManus MP, Hicks RJ, Matthews JP, et al. Positron emission tomography is superior to computed tomography scanning for response-assessment after radical radiotherapy or chemoradiotherapy in patients with non-small-cell lung cancer. *J Clin Oncol.* 2003;21:1285–1292.

Bone Marrow Transplantation (2006) 37, 617–619

www.nature.com/bmt

LETTER TO THE EDITOR

Guillain–Barre syndrome associated with rapid immune reconstitution following allogeneic hematopoietic stem cell transplantation

Bone Marrow Transplantation (2006) **37**, 617–619. doi:10.1038/sj.bmt.1705283; published online 30 January 2006

Guillain–Barre syndrome (GBS) is a rare complication following hematopoietic stem cell transplantation (HSCT), and its pathogenesis remains unclear. GBS in the early post transplant period has been attributed to the conditioning regimen, particularly cytosine arabinoside.[1] In contrast, the etiology of GBS in the late post transplant period remains unknown.[2] Some reports suggest an association with antecedent infections such as cytomegalovirus (CMV) and *Campylobacter pylori*. As few cases of GBS during acute graft-versus-host disease (acute GVHD) have been reported, acute GVHD is unlikely to be the cause of GBS.[2] We report a patient who developed GBS during rapid immune reconstitution following allogeneic HSCT.

A 34-year-old woman with acute lymphoblastic leukemia in the second remission underwent allogeneic peripheral blood stem cell transplantation from a one-antigen-mismatched related donor. The conditioning regimen comprised of cyclophosphamide and busulfan. GVHD prophylaxis was cyclosporine and short-term methotrexate. Diffuse erythema and diarrhea appeared on day 20; acute GVHD was diagnosed after skin biopsy. We initiated methylprednisolone 1 mg/kg, to which GVHD gradually responded. On day 30, she developed abdominal pain and was positive for CMV pp65 antigenemia. CMV colitis was diagnosed after colonoscopy with tissue biopsy. Her symptoms gradually improved with ganciclovir, and CMV antigenemia turned negative on day 70. On day 78, she complained of muscle weakness in the lower extremities, which progressed to quadriplegia on day 85. Muscle weakness was prominent in the proximal lower extremities. Deep tendon reflexes were absent in all the four extremities. Autonomic nervous and sensory function remained clinically normal. Magnetic resonance images of the whole spinal cord failed to show any abnormalities. Cerebrospinal fluid (CSF) showed normal levels of cell counts, protein, and glucose. CSF cultures and polymerase chain reaction using CMV-specific primers were negative. Serological tests for myasthenia gravis and anti-ganglioside antibody were also negative. Nerve conduction studies showed no conduction blocks, while the amplitudes of action potentials of compound muscle and sensory nerve were abnormally reduced. Electromyelography showed fibrillation potentials and positive sharp waves, which were consistent with denervation of muscle fibers. A sural nerve biopsy revealed axonal degeneration with infiltration of CD8+ T cells and macrophages. Based on these findings, axonal type GBS was diagnosed.

Notably, the serum IgG level rapidly increased, when the patient developed GBS (Figure 1). Electrophoresis of serum immunoglobulin revealed no clonality. Single strand conformation polymorphism (SSCP) analysis of T-cell receptor (TCR) Vβ genes amplified by the reverse transcription-polymerase chain reaction from peripheral blood mononuclear cells on day 78 showed several distinct bands of TCR Vβ genes (Figure 2). This indicates clonal expansions of T cells. SSCP analysis of peripheral blood mononuclear cells showed that some TCR clonotypes of post transplant patient T cells were identical to those of donor T cells. These findings demonstrate that donor-derived mature T cells expanded clonally in the peripheral pool when the patient developed GBS.

We initiated high-dose immunoglobulin therapy on day 88, but to no avail. Immune suppression was not intensified, and the serum concentration of cyclosporine was maintained at around 80 ng/dl. Plasma exchange was not conducted in this patient, since there is little evidence supporting its usefulness for GBS following HSCT. Her muscle strength remained unchanged from day 85 to day 148. On day 150, the patient displayed rapid recovery of muscle strength. On day 230, she could walk with assistance. She developed no symptoms of chronic GVHD. She was discharged on day 250.

The clinical course of the present patient provides important information about the pathogenesis of GBS following HSCT. She had not presented with the typical features of GBS such as an increase in CSF protein and anti-ganglioside antibodies. These findings suggest differences in the pathogenesis between GBS in the non-transplant setting and that following HSCT. A sural nerve biopsy showed infiltration of T cells and macrophages, suggesting an immune-mediated pathogenesis. GVHD was suspected to be an etiological factor in the immune-mediated pathogenesis. However, symptoms of acute GVHD had already resolved at the onset of GBS, and GBS improved without intensifying immune suppression. These findings are consistent with previous reports.[2] It is reasonable to assume that GBS following HSCT would be attributable to immune-mediated mechanisms other than GVHD.

Her clinical course suggests an association between the antecedent CMV infection and GBS. In the previous reports, two types of peripheral neuropathy owing to CMV infection have been noted: direct damage of infected neural cells and immune-mediated 'cross-reacting mechanism'.[3,4] In this patient, direct neural involvement by CMV

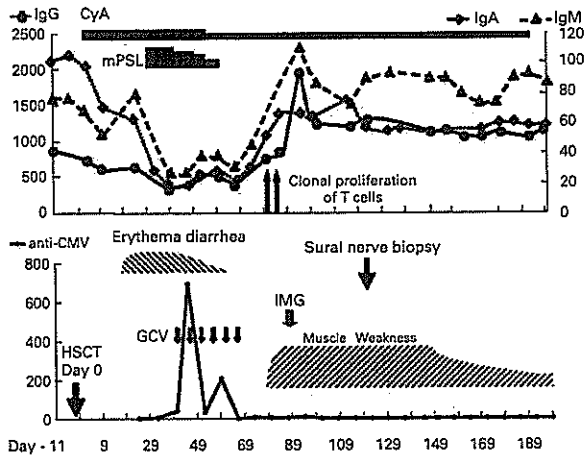

Figure 1 Clinical course of the present patient. The patient developed skin erythema and diarrhea of acute graft-versus-host disease (GVHD) on day 20, to which methylprednisolone therapy responded. Cytomegalovirus (CMV) pp65 antigenemia tested positive on day 30. After starting ganciclovir, CMV antigenemia tested negative on day 70. The patient developed muscle weakness on day 78. The development of muscle weakness was followed by clonal proliferations of mature T cells and rapid increase of serum immunoglobulin levels. Muscle weakness improved without intensifying immune suppression. CyA = cyclosporine; mPSL = methylprednisolone; anti-CMV = CMV pp65 antigenemia; IMG = high-dose immunoglobulin therapy.

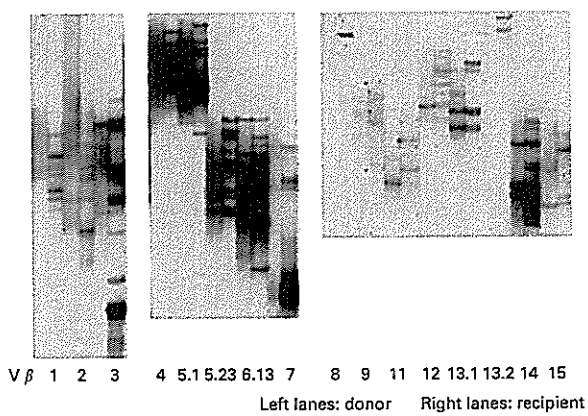

Figure 2 Single strand conformation polymorphism (SSCP) analysis of T-cell receptor (TCR) Vβ genes 1–15. SSCP analysis of TCR Vβ genes amplified by the reverse transcription-polymerase chain reaction from peripheral blood mononuclear cells on day 78 showed clonal expansions of T cells. Some TCR clonotypes of patient-derived T cells were identical to those of donor-derived T cells. Left lanes are the data of donor. Right lanes are of the patient.

was unlikely, because GBS developed after CMV antigenemia disappeared and neural symptoms resolved without anti-CMV therapy. A humorally mediated 'cross-reacting mechanism' was attributable to CMV-related GBS in a non-transplant patient.[4] This could be a possible etiology of GBS following HSCT; however, the clinical symptoms of this patient were distinct from those of CMV-related GBS in the non-transplant setting. Non-transplant patients with CMV-related GBS frequently develop sensory loss (90%), cranial nerve involvement (80%), and respiratory insufficiency (65%).[5,6] These clinical differences suggest that a humorally mediated cross-reacting mechanism was not likely in this patient.

Most notably, the development of GBS is associated with rapid immune recovery, which has been suggested as a possible cause of immune dysregulation.[7,8] In the early post transplant period, naive B cells in the marrow and mature T cells in the peripheral blood expand oligoclonally in response to antigenic stimulation such as CMV.[9] Both expanded populations of lymphocytes could contribute to the immune dysregulation.[7,8,10] Oligoclonally expanded naive B cells produce autoantibodies.[10] Peripheral expansions of mature T cells generate self-reacting T cells, possibly because proliferation is not regulated by the thymus.[7,8,10] In this patient, immunological analysis revealed clonalities of donor-derived mature T cells. A sural nerve biopsy showed infiltration of T cells and few deposits of immunoglobulins. In addition serum anti-ganglioside antibodies, the presence of which in non-transplant GBS patients is the basis for the hypothesis of humorally mediated cross reacting mechanism, were absent. Taken together with these findings, it is reasonable to assume that GBS following HSCT might be attributable to peripheral expansion of mature lymphocytes following CMV infection.

In conclusion, we describe an HSCT patient who developed proximal-dominant, axonal motor-sensory type of GBS. The patient's symptoms resolved with supportive therapy. The clinical course suggests that peripheral expansion of mature T cells following CMV infection may be an etiological factor in GBS following HSCT.

G Fujisaki[1], M Kami[1,4], N Murashige[1], Y Kishi[1], A Hori[1,4], A Chizuka[1], Y Ugawa[2], K Kobayashi[3,4] and R Tanosaki[1]

[1]*Hematopoietic Stem Cell Transplantation Unit, The National Cancer Center Hospital, Tokyo, Japan;*
[2]*Department of Neurology, Division of Neuroscience, Graduate School of Medicine, University of Tokyo, Tokyo, Japan;*
[3]*Department of Hematology, The JR Tokyo General Hospital, Tokyo, Japan and*
[4]*Division of Exploratory Research, The Institute of Medical Science, University of Tokyo, Tokyo, Japan*
E-mail: kami-tky@umin.ac.jp

References

1 Rodriguez V, Kuehnle I, Heslop HE, Khan S, Krance RA. Guillain–Barre syndrome after allogeneic hematopoietic stem cell transplantation. *Bone Marrow Transplant* 2002; **29**: 515–517.
2 Wen PY, Alyea EP, Simon D, Herbst RS, Soiffer RJ, Antin JH. Guillain–Barre syndrome following allogeneic bone marrow transplantation. *Neurology* 1997; **49**: 1711–1714.
3 Brew BJ. The peripheral nerve complications of human immunodeficiency virus (HIV) infection. *Muscle Nerve* 2003; **28**: 542–552.
4 Yuki N. Infectious origins of, and molecular mimicry in, Guillain–Barre and Fisher syndromes. *Lancet Infect Dis* 2001; **1**: 29–37.

5 Visser LH, van der Meche FG, Meulstee J, Rothbarth PP, Jacobs BC, Schmitz PI *et al.* Cytomegalovirus infection and Guillain–Barre syndrome: the clinical, electrophysiologic, and prognostic features. Dutch Guillain–Barre Study Group. *Neurology* 1996; **47**: 668–673.
6 Jacobs BC, van Doorn PA, Groeneveld JH, Tio-Gillen AP, van der Meche FG. Cytomegalovirus infections and anti-GM2 antibodies in Guillain–Barre syndrome. *J Neurol Neurosurg Psychiatry* 1997; **62**: 641–643.
7 Kojima K, Kurokawa MS, Tanimoto K, Kojima Y, Hara M, Yoshino T *et al.* Clonal expansion of limited T cell clonotypes in affected muscle from a patient with post-transplant polymyositis. *Bone Marrow Transplant* 2002; **30**: 467–470.
8 King C, Ilic A, Koelsch K, Sarvetnick N. Homeostatic expansion of T cells during immune insufficiency generates autoimmunity. *Cell* 2004; **117**: 265–277.
9 Peggs KS, Mackinnon S. Immune reconstitution following haematopoietic stem cell transplantation. *Br J Haematol* 2004; **124**: 407–420.
10 Sherer Y, Shoenfeld Y. Autoimmune diseases and autoimmunity post-bone marrow transplantation. *Bone Marrow Transplant* 1998; **22**: 873–881.

Myeloablative allogeneic hematopoietic stem cell transplantation for non-Hodgkin lymphoma: a nationwide survey in Japan

Sung-Won Kim, Tetsuya E. Tanimoto, Noriyuki Hirabayashi, Seiichi Goto, Masahiro Kami, Satoshi Yoshioka, Toshiki Uchida, Kenji Kishi, Yuji Tanaka, Akio Kohno, Masaharu Kasai, Masakazu Higuchi, Masanobu Kasai, Shin-ichiro Mori, Takahiro Fukuda, Koji Izutsu, Hiroshi Sao, Takayuki Ishikawa, Tatsuo Ichinohe, Kengo Takeuchi, Kinuko Tajima, Ryuji Tanosaki, Mine Harada, Shuichi Taniguchi, Kensei Tobinai, Tomomitsu Hotta, and Yoichi Takaue

We retrospectively surveyed the data of 233 patients who underwent myeloablative allogeneic hematopoietic stem cell transplantation (allo-HSCT) for non-Hodgkin lymphoma (NHL). Donors were HLA-matched relatives in 154 patients (66%) or unrelated volunteers in 60 (26%). Ninety patients (39%) were in complete remission. One hundred ninety-three (83%) received a total body irradiation (TBI)–based regimen, and 40 (17%) received a non–TBI-based regimen. Acute graft-versus-host disease (GVHD) occurred in 155 (67%) of the 233 evaluable patients; grade II to IV in 90 (39%), and grade III to IV in 37 (16%). Treatment-related mortality (TRM) was observed in 98 patients (42%), and 68% of them were related to GVHD. In a multivariate analysis, chemoresistance, prior autograft, and chronic GVHD were identified as adverse prognostic factors for TRM. Relapse or progression of lymphoma was observed in 21%. The 2-year overall survival rates of the patients with indolent (n = 38), aggressive (n = 111), and lymphoblastic lymphoma (n = 84) were 57%, 42%, and 41%, respectively. In a multivariate analysis, chemoresistance, prior autograft, and prior radiotherapy were identified as adverse prognostic factors for overall survival. Although myeloablative allo-HSCT represents an effective therapeutic option for patients with NHL, more work is still needed to decrease TRM and relapse. (Blood. 2006;108:382-389)

Introduction

Hematopoietic stem cell transplantation (HSCT) for patients with non-Hodgkin lymphoma (NHL) has been mainly focused on an autograft strategy. High-dose therapy with autologous HSCT (auto-HSCT) can increase remission rates and possibly prolong disease-free survival and overall survival (OS) in patients with chemotherapy-sensitive NHL at relapse.[1] This is also effective as first-line therapy for those with advanced aggressive lymphoma.[2] Nevertheless, relapse is a frequent cause of treatment failure after auto-HSCT.[1,3]

Allogeneic HSCT (allo-HSCT) has several advantages over auto-HSCT, because the former can avoid the reinfusion of malignant cells and can also be associated with a graft-versus-lymphoma (GVL) effect, which might reduce the risk of relapse. Most physicians believe that a small fraction of patients with end-stage aggressive lymphoma can still achieve prolonged lymphoma-free survival with the application of allo-HSCT. However, the high incidence of treatment-related mortality (TRM) (up to 55%) associated with allogeneic HSCT with a myeloablative regimen has prevented the wider application of this strategy.[4-8] Several reports on allo-HSCT for refractory or advanced lymphoma, as well as studies comparing auto- versus allo-HSCT for NHL, have been published over the past decade.[8-10] However, most of these studies were small and nonrandomized, and incorporated patients who had heterogeneous backgrounds. Thus, the role of allo-HSCT in the treatment of NHL remains controversial. Moreover, the outcome of allo-HSCT in each histologic subtype has not been fully determined. Previous studies have suggested that allo-HSCT improves the prognosis of patients with advanced follicular lymphoma (FL),[7,10,11] whereas few reports have been published on its benefit in aggressive lymphoma.[12,13] In particular, there has been very little information available on subtypes, including mantle-cell lymphoma[11,14]; peripheral T-cell lymphoma, unspecified (PTCL)[15]; natural killer (NK) cell lymphoma[16]; and anaplastic large cell lymphoma.

The application of reduced-intensity stem cell transplantation (RIST) or "nonmyeloablative" HSCT has been reported to decrease

From the Hematology and Hematopoietic Stem Cell Transplantation Division, National Cancer Center Hospital, Tokyo, Japan; the Department of Hematology, Tottori University Hospital, Tottori, Japan; the Department of Internal Medicine, Nagoya Daini Red Cross Hospital, Nagoya, Japan; the Department of Hematology/Oncology, Kyoto University Hospital, Kyoto, Japan; the Division of Hematology, Tokai University Hospital, Isehara, Japan; the Department of Hematology, Tokyo Metropolitan Komagome Hospital, Tokyo, Japan; the Department of Hematology and Oncology, JA Aichi Showa Hospital, Konan, Japan; the Department of Internal Medicine, Sapporo Hokuyu Hospital, Sapporo, Japan; the Department of Hematology, Hamanomachi Hospital, Fukuoka, Japan; the Department of Cell Therapy and Transplantation Medicine, University of Tokyo, Tokyo, Japan; the Department of Hematology, Meitetsu Hospital, Nagoya, Japan; the Department of Pathology, Cancer Institute of Japanese Foundation for Cancer Research, Tokyo, Japan; the First Department of Internal Medicine (Medicine and Biosystemic Science), Kyushu University Graduate School of Medical Sciences, Fukuoka, Japan; and the Department of Hematology, Toranomon Hospital, Tokyo, Japan.

Submitted March 1, 2005; accepted December 22, 2005. Prepublished online as *Blood* First Edition Paper, March 7, 2006; DOI 10.1182/blood-2005-02-0596.

Supported in part by grants from the Ministry of Health, Labor and Welfare, Japan.

Presented in part as a poster presentation at the 44th annual meeting of the American Society of Hematology, Philadelphia, PA, December 2002.

Reprints: Yoichi Takaue, Medical Oncology, National Cancer Center Hospital, 5-1-1, Tsukiji, Chuo-Ku, Tokyo 104-0045, Japan; e-mail: ytakaue@ncc.go.jp.

The publication costs of this article were defrayed in part by page charge payment. Therefore, and solely to indicate this fact, this article is hereby marked "advertisement" in accordance with 18 U.S.C. section 1734.

TRM.[17-19] Additionally, the recent development of supportive treatments may have decreased the risk of TRM and facilitated the application of allo-HSCT to NHL.[20] Therefore, we conducted a retrospective nationwide survey on Japanese patients with NHL who had undergone conventional allo-HSCT to establish a benchmark of myeloablative allo-HSCT in the treatment of NHL.

Patients, materials, and methods

Data sources

This survey collected the data of 233 consecutive patients who received myeloablative allo-HSCT for NHL between 1990 and 2001 in 56 participating hospitals. Data were derived from questionnaires distributed to each hospital. Additional questionnaires were sent to confirm the follow-up data, including the occurrence of graft-versus-host disease (GVHD). The indications for allo-HSCT were left to the discretion of each institution. The patients included in this study received a conditioning regimen with an intensity that was equivalent to that of total body irradiation (TBI) plus cyclophosphamide or busulfan plus cyclophosphamide. Patients who had previously received monoclonal antibody therapy or T-cell–depleted transplantation, those younger than 14 years, and those who received RIST were not included. Additionally, those with adult T-cell leukemia/lymphoma were excluded because their clinical course differed from that of other types of lymphoma. The minimum data required for the inclusion of a patient in this study were age, sex, histologic diagnosis, prior treatment details, status at transplantation, donor information, conditioning regimen, date of transplantation, therapy-related complications, date of last follow-up, disease status at follow-up, date of disease progression/death, and cause of death. Approval was obtained from the institutional review board. Informed consent was provided according to the Declaration of Helsinki.

Definitions

The initial institutional histologic diagnosis was further reviewed by a pathologist (K. Takeuchi) using the WHO classification.[21] Briefly, NHL was divided into 3 clinical subtypes: indolent, aggressive, and lymphoblastic lymphoma. Indolent lymphoma included all grades of FL and extranodal marginal zone B-cell lymphoma of mucosa-associated lymphoid tissue (MALT lymphoma). Aggressive lymphoma included all lymphomas except for indolent and lymphoblastic lymphoma. Transformed indolent lymphoma and Burkitt lymphoma were classified as aggressive lymphoma. Furthermore, because most of the patients were evaluated before publication of the WHO classification, this analysis only included those who had tumors that formed lesions, such as T-cell lymphoblastic lymphoma (T-LBL), and all other patients who had features of leukemia were excluded. Those with chemosensitive disease included all patients who had shown a response to the last chemotherapy prior to transplantation (partial remission [PR], complete remission [CR] unconfirmed, and CR), whereas chemoresistant disease included those with primary refractory disease or refractory relapse prior to transplantation. Acute and chronic GVHD was graded according to the consensus criteria.[22,23] Patients who survived 100 days were evaluable for the assessment of chronic GVHD. OS was measured as the time from the day of transplantation until death from any cause, and progression-free survival (PFS) was the time from the day of transplantation until disease progression (PD)/relapse or death from any cause. Patients who died from transplantation-related causes were classified as TRM regardless of their disease status.

Statistical analysis

OS and PFS were calculated using the Kaplan-Meier method.[24] Surviving patients were censored on the last day of follow-up, in July 2002. The associations among patient-, disease-, and transplantation-related factors and OS were assessed by using univariate and multivariate Cox proportional hazards models. The associations between these factors and TRM were assessed by using univariate and multivariate logistic models. The variables analyzed included age, clinical subtype, histologic diagnosis, chemosensitivity, history of autograft or radiotherapy, years of transplantation, donor, source of stem cells, TBI-containing regimen, GVHD prophylaxis, and acute and chronic GVHD. Acute GVHD was treated as a time-dependent covariate in the Cox model. Stepwise variable selection at a significance level of .05 was used to identify covariates associated with outcomes. TRM and disease progression/relapse were calculated by using cumulative incidence. The statistical analysis was performed with the SAS 8.2 program package (SAS Institute, Cary, NC).

Results

Patients' characteristics

The patients' characteristics are listed in Table 1. All patients were younger than 60 years at the time of transplantation, with a median age of 31 years. Thirty-eight patients (16%) had indolent lymphoma, 111 (48%) had aggressive lymphoma (diffuse large B-cell, n = 44; PTCL, n = 22; extranodal NK/T-cell, n = 19; anaplastic large cell, n = 7; mantle cell, n = 5; Burkitt, n = 4; angioimmunoblastic T cell, n = 2; blastic NK cell, n = 2; hepatosplenic T-cell, n = 2; subcutaneous panniculitis like T cell, n = 2; mycosis fungoides with visceral dissemination, n = 2), and 84 (36%) had lymphoblastic lymphoma. Ninety patients (39%) were in CR, 38 (16%) were in PR, 42 (18%) were in primary refractory, and 63 (27%) had refractory relapse at the time of allo-HSCT. Ninety patients (39%) had received 4 or more chemotherapy regimens before allo-HSCT. Forty patients (17%) had received prior autograft, and 81 (35%) had received prior radiotherapy. One hundred fifty-four patients (66%) received a transplant from a human leukocyte antigen (HLA)–matched related donor, 19 (8%) from a 1-antigen–mismatched related donor, 43 (19%) from a matched unrelated donor, and 17 (7%) from a 1-antigen–mismatched unrelated donor. One hundred fifty-nine (68%) patients received bone marrow (60 from an unrelated donor) and 70 (30%) received granulocyte colony-stimulating factor (G-CSF)–mobilized peripheral blood. One hundred ninety-three patients (83%) received TBI-based myeloablative regimens, including TBI 12 Gy plus cyclophosphamide (n = 60); a combination of TBI, cyclophosphamide, and etoposide (n = 47); or TBI, cyclophosphamide, and cytarabine (n = 40). Forty patients (17%) received a non–TBI-based myeloablative regimen, including a combination of busulfan and cyclophosphamide with or without other agents (n = 27); melphalan, thiotepa, and busulfan (n = 3); cytarabine, ranimustine, carboplatin, cyclophosphamide, and total lymphoid irradiation (n = 2); or cytarabine, etoposide, and busulfan (n = 2). The remaining 6 patients received individualized regimens. GVHD prophylaxis included a combination of cyclosporin and methotrexate in 204 (88%) or tacrolimus and methotrexate in 22 (9%). Two hundred twenty-six patients (97%) were treated with G-CSF, starting at days +1 to +6 after graft infusion until engraftment.

GVHD

Acute GVHD occurred in 155 (67%) of the 233 patients: grade I in 65 (28%), grade II to IV in 90 (39%), and grade III to IV in 37 (16%) patients. Of the 165 patients who survived the initial 100 days after allo-HSCT, chronic GVHD occurred in 79 (48%), with extensive type in 48 (29%). In allo-HSCT from related (n = 173) and unrelated (n = 60) donors, grade II to IV acute GVHD occurred, respectively, in 61 (35%) and 30 (50%), grade III to acute GVHD occurred in 25 (15%) and 12 (20%), chronic GVHD occurred in 54 (31%) and 25 (42%) patients, and chronic extensive